

Original Article

Interaction between decadal-to-multidecadal oceanic variability and sudden stratospheric warmings

Blanca Ayarzagüena,^{1,a}  Elisa Manzini,^{2,a}  Natalia Calvo,¹  and Daniela Matei²¹Departamento de Física de la Tierra y Astrofísica, Universidad Complutense de Madrid, Madrid, Spain. ²Max-Planck-Institut für Meteorologie, Hamburg, Germany

Address for correspondence: Blanca Ayarzagüena, Departamento de Física de la Tierra y Astrofísica, Universidad Complutense de Madrid, 28040 Madrid, Spain. bayarzag@ucom.es

Major sudden stratospheric warmings (SSWs) are the most important phenomena of the wintertime boreal stratospheric variability. During SSWs, the polar temperature increases abruptly, and easterlies prevail in the stratosphere. Their effects extend farther from the polar stratosphere, affecting near-surface circulation. According to observations, SSWs are not equally distributed in time, with decades experiencing very few events, while others experiencing SSWs almost every winter. Some sources of this SSW multidecadal variability can be traced back to sea surface temperature changes. Here, we investigate the effects of Pacific decadal variability (PDV) and Atlantic multidecadal variability (AMV) on SSWs. We use for the first time a large ensemble of historical experiments to examine the modulation of the frequency, tropospheric precursors, and impact of SSWs by the PDV and AMV. We find a strong impact of the PDV on the occurrence of SSWs, with a higher SSW frequency for the positive phase of the PDV. This PDV influence is mediated by constructive interference of PDV anomalies with tropospheric stationary waves. The main effect of AMV is, instead, a modulation of the tropospheric response to SSWs, a finding that can be useful for predicting the tropospheric fingerprint of SSWs.

Keywords: multidecadal variability; sudden stratospheric warmings; Pacific decadal variability; Atlantic multidecadal variability

Introduction

Major sudden stratospheric warmings (SSWs) are one of the most dramatic phenomena of atmospheric variability. SSWs consist of abrupt warming of the polar stratosphere and a subsequent breakup of the stratospheric vortex.¹ They are caused by the dissipation of Rossby waves that propagate upward from the troposphere.² SSW effects are not only limited to the stratosphere but also extend to the troposphere (Ref. 2 and Refs. therein) and even affect sea surface temperatures (SSTs)³ and Arctic sea ice.⁴

On the basis of the observational record (since 1958) and considering events defined by the rever-

sal of the winds at 60°N and 10 hPa, SSWs occur approximately every two winters but are not equally distributed over time.⁵ While only two events were detected in the 1990s, almost every winter in the 2000s experienced an SSW event. This may be indicative of the multidecadal variability of SSWs.⁶ Indeed, a few modeling studies have suggested the existence of low-frequency variability of SSWs.^{7,8} However, the short observational data record does not allow the full characterization of their long-term variability. In addition, other issues have arisen, such as the computational cost of running long simulations using models with a well-resolved stratosphere and the storage required for the daily output needed for the identification of SSWs. All these reasons have made this topic scarcely investigated.

^aThese authors contributed equally to this study.

Very little is also known about the sources of the multidecadal variability of SSWs. There is some indication that they should be primarily located in the ocean, and more specifically, related to decadal-to-multidecadal variability of SSTs, as it can modify the atmospheric state and, in turn, the generation and upward propagation of wave activity. Indeed, some authors have revealed a connection between the Pacific decadal variability (PDV) and changes in the polar vortex.^{9–12} A positive phase of PDV (PDV⁺) leads to a weakening of the polar vortex, as shown by both reanalysis^{10,12} and modeling studies.^{11,12} The results are consistent with Refs. 13–15, who investigated the effects of prescribed SST anomalies in the North Pacific on the atmosphere. In agreement with mean polar vortex changes, PDV⁺ was found to increase the frequency of SSWs, with, however, contrasting results on the statistical significance of this impact.^{10,11} In addition, the PDV signal might be contaminated by the El Niño–Southern Oscillation (ENSO).¹⁶ Ref. 11 compared the frequency of SSWs during PDV phases regardless of the ENSO phase or during ENSO neutral conditions. In both cases, the likelihood of SSWs was higher with PDV⁺ than with PDV⁻, but the size of samples was small, and so, the statistical significance of the results was limited. Instead, Ref. 12 found an increase in the SSW frequency for PDV⁺ only when the ENSO signal was not removed.

Further SST variability with potential impact on the polar stratosphere could be related to the Atlantic multidecadal variability (AMV). However, fewer efforts have been devoted to this teleconnection compared with the PDV, and large uncertainties remain regarding the AMV impact on SSWs. Ref. 7 related low-frequency SST variability to changes in heat flux from the ocean into the atmosphere in the North Atlantic region. Refs. 17–19 suggested that warm anomalies in the Atlantic Ocean associated with a positive phase of the AMV (AMV⁺) induce anomalous warming in the polar stratosphere in early and midwinter in high-top models. Ref. 20 identified a relation of the same sign between AMV and polar stratospheric changes in reanalysis data, but in this case, it occurred in late winter. All these studies used monthly data and so, they could not investigate AMV effects on SSWs. Only Ref. 15 investigated these effects on the frequency of SSWs, but in idealized experiments with a

prescribed AMV⁺ phase or a combined AMV⁺ and PDV⁺ phase. A slight increase in the frequency of SSWs was found for AMV⁺, much weaker than that for PDV⁺.

The goal of our study is to examine the impact of the two main modes of low-frequency SST variability in the Pacific and Atlantic Oceans, PDV and AMV respectively, on SSWs. To do so, we use for the first time a large ensemble of model simulations, allowing not only for the characterization of the effects of each phenomenon separately but also for the combination of both. Moreover, our SSW analysis concerns not only their frequency, as previous studies did, but we also try to answer the question of whether long-term SST variability modulates tropospheric precursors and response to SSWs.

Materials and methods

Model and experiments

In this study, we analyze daily outputs of an ensemble of the 95 realizations of the historical experiment performed with the Max Planck Institute (MPI) Earth System Model 1.1. (MPI-ESM1.1) model, part of the MPI Grand Ensemble (MPI-GE).²¹ The MPI-ESM1.1 is a coupled atmosphere–ocean–sea ice model.²² Here, we use outputs from the atmospheric component, the ECHAM6 model at T63L47 resolution, that is, with a spherical truncation of T63 and 47 hybrid levels up to 0.01 hPa (~80 km). Given the relatively low vertical resolution, the Quasi-Biennial Oscillation (QBO) is not explicitly simulated.²³ In addition, no QBO nudging is employed in MPI-ESM1.1. For further detailed description, please see Ref. 21.

The historical experiment extends from 1850 to 2005 and includes observed transient natural and anthropogenic forcings and natural variability following the Coupled Model Intercomparison Project phase 5 (CMIP5) recommendations.²⁴ More specifically, ozone concentrations and volcanic aerosol forcing are prescribed on the basis of Ref. 25 and the dataset from Ref. 26, respectively (see more information in the supplementary material of Ref. 27, online only). The 95 realizations are initialized from different years of a 2000-year experiment using fixed preindustrial radiative forcing.

Methods

Computation of anomalous fields and filtered series. Anomalous fields are computed separately

for each ensemble member on the basis of its own climatology. The global warming signal in geopotential height (Z) anomalies is removed by subtracting the global mean of the field at each time step.²⁸ The use of Z anomalies is two-fold, and so, the filtering applied to the anomalies is different. When studying the possible modulation of tropospheric precursors and response to SSWs by PDV and AMV, we analyze the 8-day low-pass filtered geopotential height anomalies at 500 hPa (Z_{500}) for 10 days before and 30 days after the central date of SSWs during PDV and AMV phases, respectively. The 8-day low-pass filter is applied to retain only quasistationary circulation anomalies as we seek persistent tropospheric anomalies, such as blocking highs or persistent cyclonic anomalies.²⁹

In the analysis of the potential influence of the atmospheric mean state during the PDV or AMV phase on the occurrence of SSWs, we apply a 10-year low pass filter to anomalous Z data at different levels so that the variability of higher frequency that might contaminate the results is removed. To perform this analysis, seasonally averaged outputs over December–January–February (DJF) are employed. The selection of these 3 months is based on two reasons. DJF correspond to midwinter when wave activity is typically at its maximum,³⁰ and so, the occurrence of SSWs is more likely. Second, it is when the main differences in the occurrence of SSWs depending on the PDV and AMV phases are identified, as shown in Results Section. In the case of SST anomalies, the detrending is performed by removing only the global area average outside the poles (60°S – 60°N) to avoid the effects of changes in sea ice extension.³¹ Furthermore, a 10-year low-pass filter has been applied to only retain the multidecadal variability of SSTs. In this case, this filter serves to remove the typical signal associated with ENSO.

Identification of SSW events. The SSW events are identified using the standard wind reversal definition³² with the additional constraint of selecting only events longer than 5 days. The zonal wind reversal definition is applied to daily zonal mean zonal winds at 10 hPa, 60°N and selects episodes of easterly zonal mean winds for the extended Northern winter season, from November to March. The additional constraint on the event duration is motivated by the modeled zonal winds, which are biased

low in strength. Consequently, the modeled SSW frequency is overestimated, especially in November and December.³³ Moreover, this bias favors the occurrence of short and shallow events,³⁴ which are not of dynamical interest because they do not contribute to stratosphere-to-troposphere downward coupling.³⁵ Applied to the reanalysis record, the wind reversal definition with the additional constraint on the event duration, indeed, selects only the events denoted as “downward propagating” by Ref. 35, and reduces the observed SSW frequency to ~ 0.4 event/year. As will be shown in Results Section, the model rate of SSWs is close to this observed value. The zonal wind field used in the SSW calculation and the analysis of the atmospheric mean state for PDV and AMV phases is not detrended because the thermal signal from increased greenhouse gas concentrations for this dynamical field over the historical period is negligible (not shown).

Long-term SST variability indices. PDV is defined as the first empirical orthogonal function of monthly SST anomalies in the extratropical North Pacific (120° – 280°E , 20° – 60°N , see Ref. 36). As mentioned before, to remove the possible ENSO signal in the PDV index, a 10-year low-pass filter is applied to SST anomalies. AMV is computed as 10-year low-pass filtered annual mean area-averaged SST anomalies over the North Atlantic Basin (80°W – 0°E , 0° – 60°N , see Ref. 31). Unfiltered AMV and PDV indices are also retained as they are used to define extreme PDV and AMV, as indicated below. Winters (November–March) with the absolute value of the seasonal averaged PDV index above 1 standard deviation are considered as potential extreme PDV events. Potential extreme AMV events are chosen in the same way, but in this case based on an annual average index, with the annual average defined for each year from July to the following June. Extreme PDV and AMV events are finally selected when the unfiltered index for extreme events is of the same sign as the filtered index. This procedure ensures that SSWs, which are identified using unfiltered data, are not triggered by seasonal SST anomalies of opposite sign to low-frequency PDV or AMV phases. Composite maps of different variables are built for these extreme events to characterize the associated changes in fields during each phase of PDV or AMV. Once the extreme events are identified and field anomalies

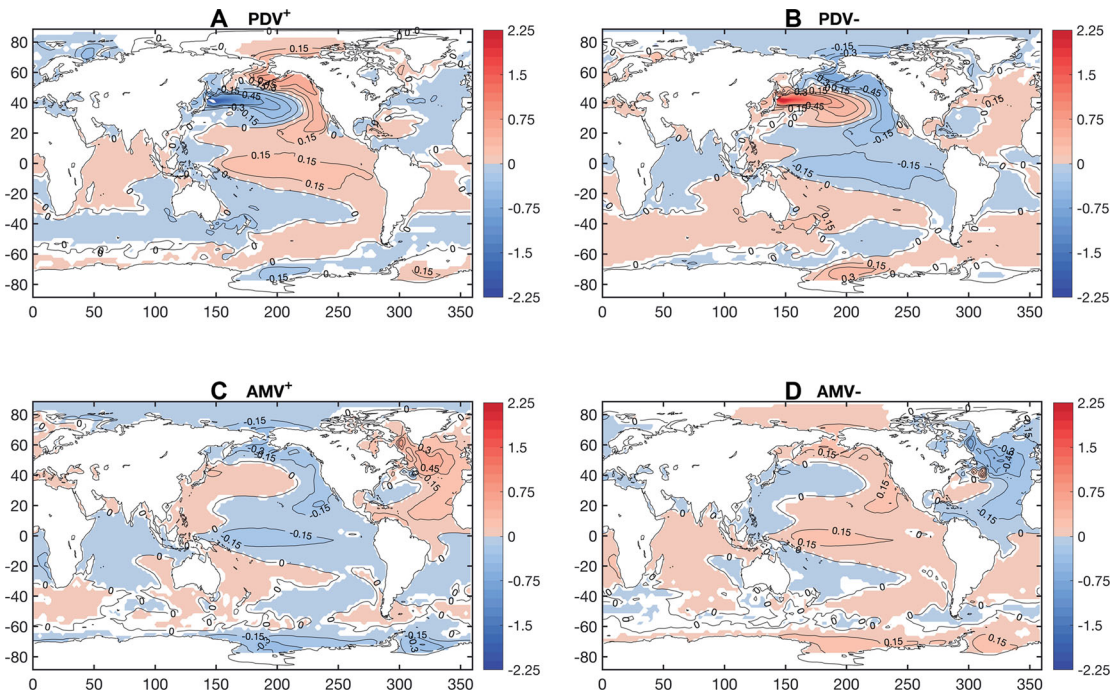


Figure 1. Characterization of the PDV and AMV in the MPI-ESM1.1 model. Composite maps of anomalous annual SSTs for filtered (A and B) PDV and (C and D) AMV phases. Contour interval: 0.15 K. Shading denotes statistically significant anomalies at a 95% confidence level.

are computed, the composite maps and statistics are calculated, pooling together events from all the considered years and ensemble members. Results are almost identical to considering each member separately and then performing an ensemble mean.

Statistical tests. Results include statistical significance to provide robustness to the conclusions. To do so, two-tailed Student’s *t*-tests are applied to compute the statistical significance of anomalous fields in composite maps.³⁷ Concerning the frequency of SSWs under different oceanic conditions, the statistical significance is derived from the location of the endpoints of the notches within a box plot. The notch extremes are computed following Eq. (1):

$$\begin{aligned}
 \text{top_end} &= q_2 - \frac{1.57 \cdot (q_3 - q_1)}{\sqrt{n}} \text{ and} \\
 \text{bottom_end} &= q_2 + \frac{1.57 \cdot (q_3 - q_1)}{\sqrt{n}}, \quad (1)
 \end{aligned}$$

where q_2 is the median, q_1 and q_3 are the 25th and 75th percentiles, respectively, and n is the size of

the sample. Given the width of the notches, if two notches of two samples do not overlap, the medians of these two samples are statistically significantly different at a 95% confidence level. This statistical test is analogous to the *t*-test used for the difference of means.³⁸

PDV and AMV in the MPI-ESM1.1 model. To evaluate the ability of the MPI-ESM1.1 model to reproduce PDV and AMV patterns, we show composite maps of anomalous SSTs for PDV and AMV phases (Fig. 1). Indeed, both variability modes are reproduced reasonably well by the model. Both PDV and AMV are characterized by a horseshoe pattern in their respective basins. These features agree well with the characteristics of both phenomena in observations.^{31,36} Interestingly, significant anomalies of SST are not only present in the oceanic basin of the phenomena but also in other basins. For instance, apart from positive SST anomalies in the North Atlantic, AMV⁺ is accompanied by a PDV⁻ pattern in the North Pacific Ocean, that is, a horseshoe pattern with cold anomalies close to the American west coast and warm anomalies in

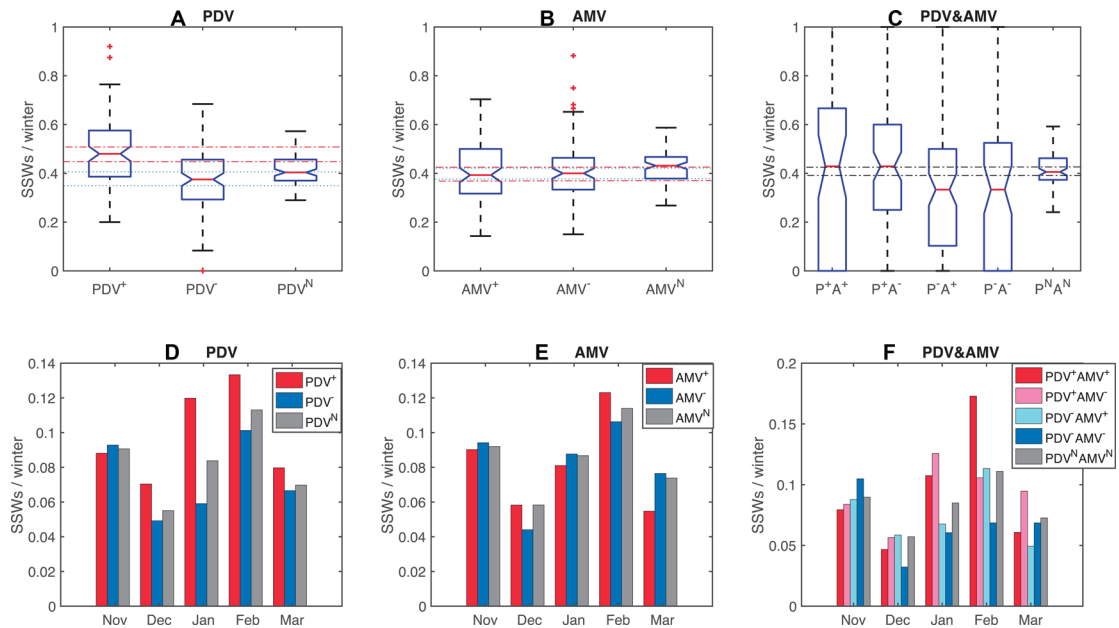


Figure 2. Impact of the PDV and AMV on the occurrence of SSWs. (A) Box plot showing the distribution of annual SSW frequency for the PDV phases. The box is bounded by the upper and lower quartiles and contains 50% of the data (the interquartile range). Whiskers indicate the maximum and minimum points in the distribution that are not outliers. Outliers (red crosses) are defined as points with values greater than 3/2 times the interquartile range from the ends of the box. Red dashed-dotted (blue dotted) lines limit the confidence interval, as defined by the extremes of the notches, of the median value (horizontal red bar) for the positive (negative) PDV phase. (B) Same as A but for the AMV. (C) Same as A but for different combined PDV and AMV phases, and the confidence interval is reported only for the neutral phase. (D) Seasonal distribution of SSWs by month for the PDV phases. (E and F) Same as D but for the AMV and combined PDV and AMV phases, respectively.

the central North Pacific. In the case of the PDV, interhemispheric differential warming is detected in the Atlantic sections. Indeed, the numbers of combined extreme PDV and AMV events of the same sign (PDV⁺AMV⁺ (214) and PDV⁻AMV⁻ (248)) are about half the number of PDV and AMV extreme events of different sign (PDV⁺AMV⁻ (549) and PDV⁻AMV⁺ (547)). Similar aliasing between opposed phases of PDV and AMV has already been discussed in the literature (e.g., Refs. 39 and 40), but there is no full consensus about the existence of this interbasin linkage at a decadal timescale.

Results

Mean frequency and seasonal distribution of SSWs

First, we analyze the PDV and AMV influence on the occurrence of SSWs. Statistically significantly higher frequency of SSWs in winter is detected for the PDV⁺ phase than for PDV⁻ and neutral PDV (PDV^N) conditions (Fig. 2A). This PDV effect on SSWs takes place mainly in January when the largest

differences in the frequency of SSWs for the PDV phases are found (Fig. 2D). Conversely, AMV does not seem to affect the occurrence of SSWs. The SSW frequency during AMV⁺ is not statistically significantly different from either AMV⁻ or AMV^N (Fig. 2B). The seasonal distribution of SSWs for the AMV phases confirms the lack of impact of AMV on the occurrence of SSWs (Fig. 2E). Only SSWs in February might seem to show a fingerprint of AMV with a higher frequency of SSWs for AMV⁺, although it is not significant (not shown). These main conclusions do not change when selecting extreme PDV and AMV events on the basis only of unfiltered PDV and AMV indices. To ensure the independence of these results from ENSO, the analysis has been repeated, including only winters under neutral ENSO conditions (values of the El Niño 3.4 index between -1 and 1 standard deviation). Once again, the conclusions do not change (not shown).

Regarding the combined PDV/AMV effects, SSW frequencies during PDV⁺AMV⁺ and PDV⁺AMV⁻ phases are close to the SSW frequency during both

PDV^N and AMV^N (Fig. 2C). Under PDV⁻AMV⁺ and PDV⁻AMV⁻, the SSW frequency is lower than under neutral conditions, but the median is not statistically significantly different from the frequency under neutral conditions. Similar to the individual PDV and AMV effects on SSWs, the largest differences in the combined cases are also found in January and February. When stratified by the AMV phase, the PDV is confirmed to strongly influence SSW frequency, especially in January (Fig. 2F).

Tropospheric circulation before and after the occurrence of SSWs

As a second step, we answer the question of whether AMV and PDV background states modulate the tropospheric precursors and response to SSWs.

The composite maps of anomalous Z500 for neutral PDV and AMV conditions (Fig. 3C, F, I, and L) before and after SSWs are, respectively, very similar. They all show that the model is able to simulate the typical tropospheric precursors and response to SSWs that have already been identified in observations (e.g., Refs. 41–43). The precursory signal of SSWs consists of two main centers of anomalies: anticyclonic anomalies over Northeastern Europe and cyclonic anomalies over the North-western Pacific, the latter being the strongest one (Fig. 3C and I). After SSWs, a negative phase of the northern annular mode is simulated with the strongest anomalies over the North Atlantic sector, matching the same phase of the North Atlantic Oscillation (NAO) in that sector (Fig. 3F and L).

Once we have evaluated the ability of the model to simulate anomalous tropospheric circulation surrounding SSWs, the modulation of these anomalies by PDV and AMV is explored. The main effect of PDV on the circulation is over the Pacific sector, as expected from the PDV SST pattern that shows the strongest anomalies in the Pacific Basin (Fig. 1A and B). Before and after SSWs, negative (positive) anomalies of Z500 are seen over the Pacific for the PDV⁺ (PDV⁻) phase with respect to PDV^N (Fig. 3A, B, D, and E). Actually, the PDV⁺ minus PDV^N pattern of Z500 resembles that of a positive phase of the Pacific North American pattern⁴⁴ and the opposite for PDV⁻ minus PDV^N. The implications for the tropospheric patterns of this influence are different, depending on the timing with respect to SSWs. In the 10 days before SSWs, PDV⁺ (PDV⁻) leads to an intensification (weakening) and an eastward

(westward) shift of the anomalous cyclone over the Western Pacific (Fig. 3A and B). Following SSWs, the amplitude of the anomalies in the pattern of PDV influence over the Pacific is comparable with that before SSWs and stronger than the anomalies of the tropospheric response to SSWs in that sector (Fig. 3D–F). In addition, the PDV modulation of the tropospheric response to SSWs is also reminiscent of the annular mode. However, the anomalies over the Atlantic Basin are not located over the main centers of action of the response to SSWs. Thus, the PDV may not modulate the tropospheric response to SSWs in that region significantly.

The AMV impact on tropospheric circulation surrounding the occurrence of SSWs is, in general, weaker than that of PDV and, when relevant, is mainly centered over the Atlantic Basin. This again agrees well with the location and intensity of the AMV-related SST pattern (Fig. 1C and D). The AMV⁺ minus AMV^N and AMV⁻ minus AMV^N patterns for 10 days before the central date of SSWs are rather weak when compared with the precursor anomalies for neutral conditions (Fig. 3G and H). Conversely, over the North Atlantic, the tropospheric response to SSWs is strongly modulated by the AMV. The AMV effects resemble an NAO pattern, although with a meridional shift (Fig. 3J and K). In particular, the negative (positive) phase of this NAO-like pattern during 30 days after SSWs is mostly found under AMV⁺ (AMV⁻), leading to a reinforced (weakened) SSW signal in the troposphere.

Given the occurrence of preferred combinations of the AMV and PDV phases of opposite sign, the previous analysis has also been performed for combined AMV/PDV phases. The main effect of PDV is imprinted on the circulation of the Pacific sector before and after the occurrence of the SSW, as negative Z500 anomalies are identified over the Western Pacific for all composites under PDV⁺ (Fig. 4A, B, F, and G) and the opposite under PDV⁻ (Fig. 4C, D, H, and I) conditions. By contrast, the AMV influence appears on the Atlantic Basin preferably when the AMV and PDV have opposite phases, in the form of a positive NAO-like pattern during PDV⁺AMV⁻ (Fig. 4B and G) and a negative NAO-like pattern during PDV⁻AMV⁺ (Fig. 4C and H). Each of these patterns is more pronounced at 30 days after SSWs. In addition, comparing Figures 3 and 4, we can deduce that the signals over the Atlantic for PDV

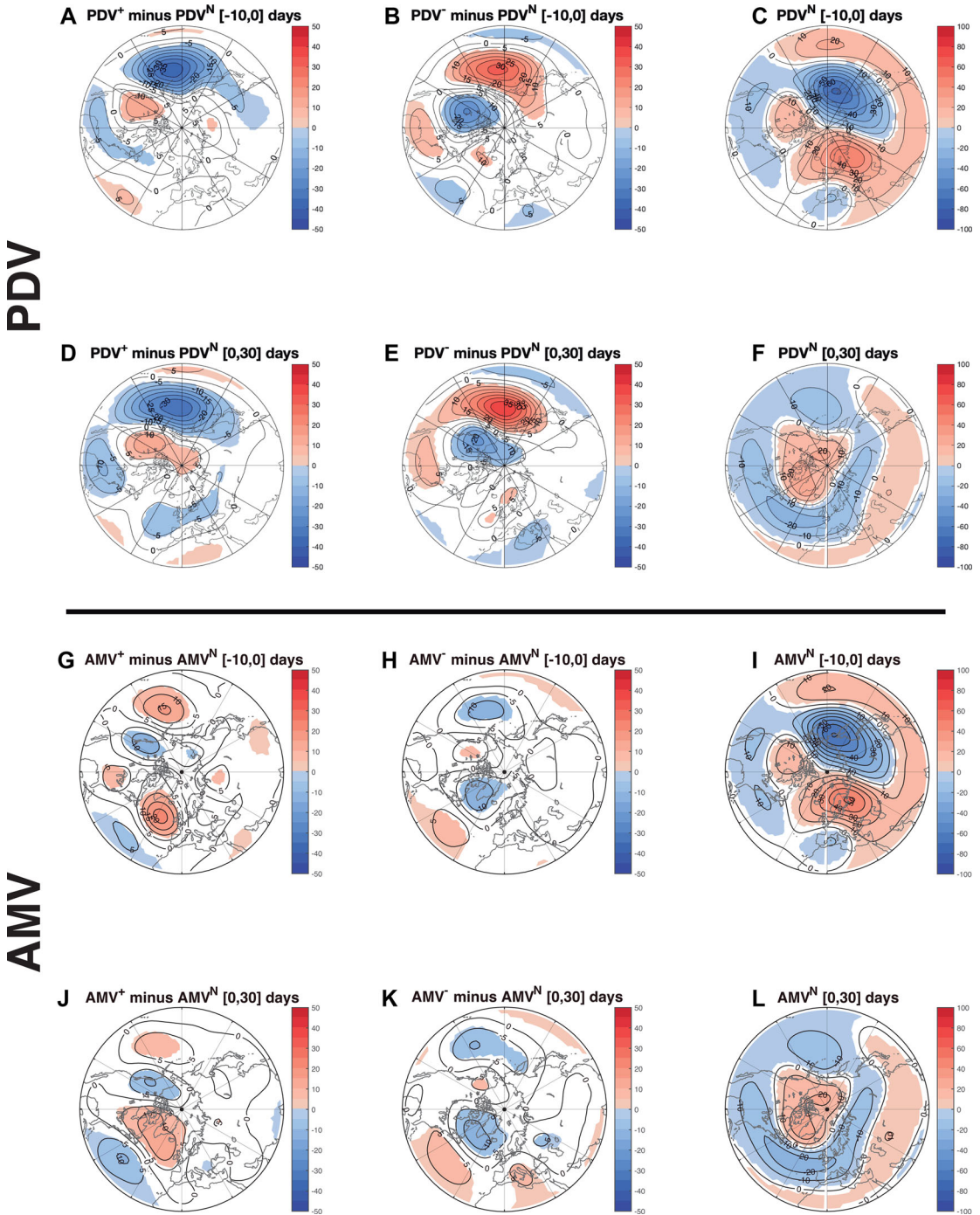


Figure 3. Modulation of tropospheric precursors and response to SSWs by the PDV and AMV. (A–C) Composite maps of detrended 8-day low-pass filtered geopotential height anomalies at 500 hPa for [–10,0] days before SSWs for PDV⁺ minus PDV^N and PDV[–] minus PDV^N and for PDV^N only. (D–F) Same as (A–C) but for [0,30] days after SSWs. Contour interval: 5 m (A, B, D, and E) and 10 m (C and F). Shading indicates statistically significant values at a 95% confidence level. (G–L) Same as (A–F) but for the AMV.

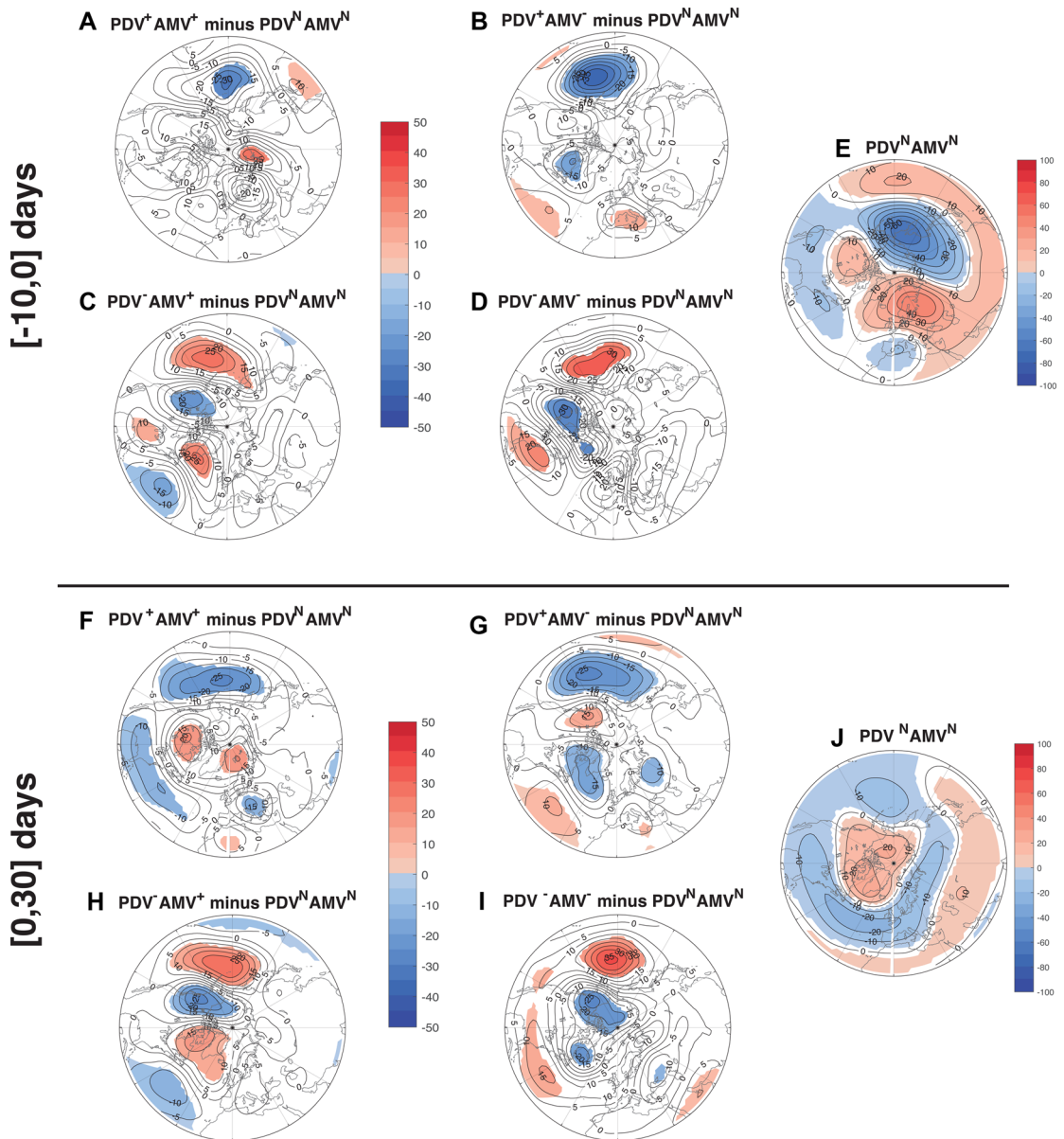


Figure 4. Modulation of tropospheric precursors and response to SSWs by the combination of the PDV and AMV. Same as Figure 3 but for different combined PDV and AMV phases.

and over the Pacific for AMV are likely explained by the preference of concurrent phases of AMV and PDV of opposite sign in the MPI-GE.

Modulation of the occurrence of SSWs by long-term SST variability

To explain how the oceanic low-frequency variability can modulate the occurrence of SSWs, we exam-

ine the atmospheric mean state for the PDV and AMV phases in winter.

The tropospheric signal of the PDV is characterized by a wave train in the Pacific–North American region. In particular, the difference between the PDV phases consists of negative anomalies over the North Pacific region and positive anomalies over Northwestern America (Fig. 5A). This dipole of

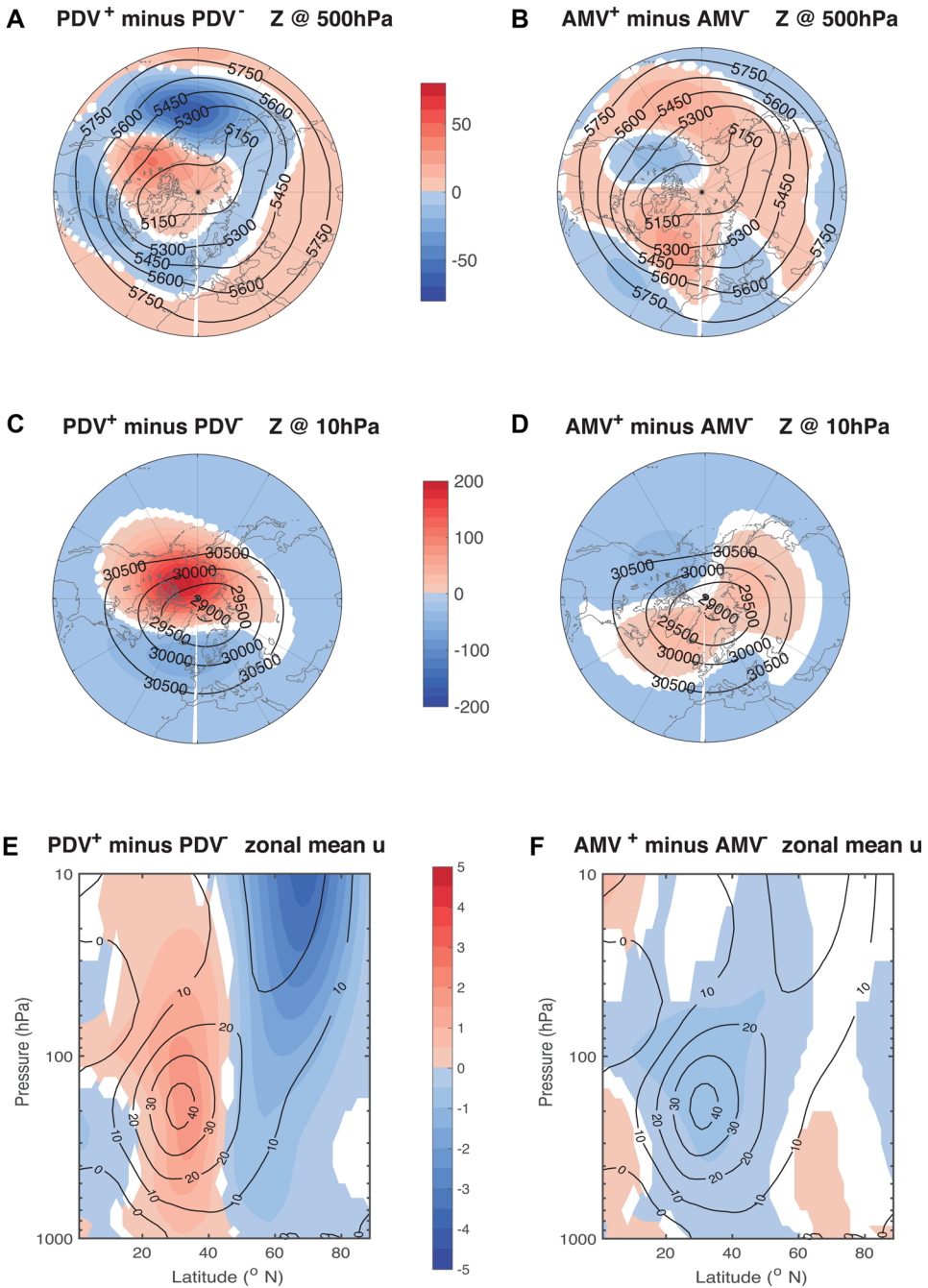


Figure 5. Modulation of the mean atmospheric state by the PDV and AMV. Differences of (left) PDV and (right) AMV phases of different 10-year low-pass filtered fields in DJF in shading: (A and B) geopotential height at 500 hPa (m), (C and D) geopotential height at 10 hPa (m), and (E and F) zonal mean zonal wind (m s^{-1}). Shading is only seen when differences are statistically significant at a 95% confidence level. Contours correspond to the climatological field in DJF.

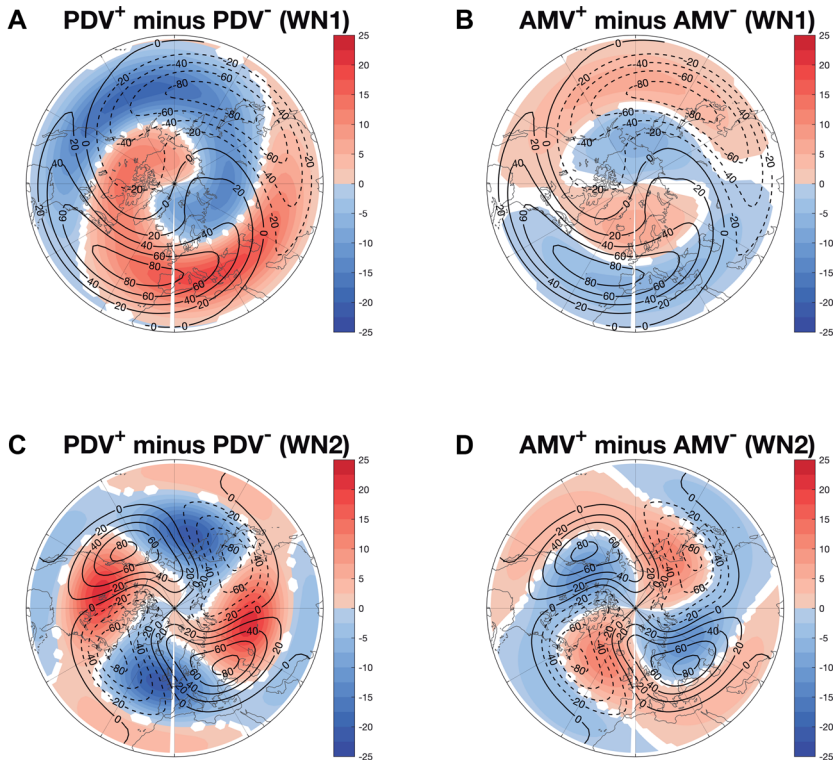


Figure 6. Modulation of the mid-tropospheric wave activity by the PDV and AMV. (A) The PDV⁺ minus PDV⁻ composite map of the anomalous WN1 wave of the Z500 in DJF in shading (interval: 2.5 m). Only statistically significant differences at a 95% confidence level are plotted. Contours correspond to the climatological WN1 of the Z500 in DJF (contour interval: 20 m). (B) Same as A but for the AMV⁺ minus AMV⁻ phases. (C and D) Same as A and B but for the WN2 wave.

anomalies in the Pacific–American area is also coincident with Z500 anomalies in that region before the occurrence of SSWs (neutral PDV or AMV phases, i.e., Fig. 3C and I). Furthermore, significant anomalies of Z500 are also detected over the Atlantic but much weaker than those over the Pacific, explaining why the North Atlantic tropospheric response to SSWs is barely affected by the PDV.

The tropospheric pattern of PDV, therefore, explains its modulation of the frequency of SSWs. The intensification of the Aleutian low is an SSW precursor related to the intensification of wavenumber-1 (WN1) wave through constructive interference,⁴⁵ mainly on the eastward side of the low (Fig. 6A). Enhanced WN1 wave activity is consistent with a weaker polar vortex shifted toward Eurasia (Fig. 5C) and, in general, with a weaker polar night jet (Fig. 5E) for PDV⁺ with respect to PDV⁻. More specifically, since the amplitude of climatological WN1 wave reaches its maximum in January (not shown), the intensification of the WN1

wave amplitude discussed above can also explain an increase in the frequency of SSWs in January during PDV⁺ (Fig. 2D). The effects of PDV on WN2 wave activity are negligible, though as the anomalous and the climatological WN2 waves are in quadrature (Fig. 6C).

Concerning the AMV, the atmospheric signal in the middle troposphere is, in general, weaker than that of the PDV. The spatial pattern is also different with stronger anomalies over the Atlantic than over the Pacific so that it projects on a negative phase of NAO for AMV⁺ (Fig. 5B). The weak anomalies of Z500 over the Pacific (Fig. 5B) and the easterly response of the tropospheric subtropical jet (Fig. 5F) are consistent with the preferred occurrence of opposed PDV and AMV phases. The weak AMV influence on the mean tropospheric state and especially on the main precursors of SSWs (Northwestern Pacific and Northeastern Europe) is consistent with the insignificant AMV influence on the frequency of SSWs (Fig. 2). Indeed, the

modulation of the polar night jet by the AMV does not show a clear and significant signal (Fig. 5D and F). In the troposphere, anomalous WN1 and WN2 waves of Z500 are, respectively, out of phase with respect to their climatology (Fig. 6B and D), suggesting destructive interference, which would hamper a vortex weakening.

Finally, the comparison of Figures 3 and 5 shows that the PDV or AMV influences on the atmospheric background state are consistent with their respective modulations of the tropospheric precursors and impacts of SSWs. To test the linearity of these modulations, the precursor and impact composites are recomputed using anomalies with respect to the mean of each particular PDV and AMV phase (Fig. 7). We find that by removing the mean PDV influence, there are still some differences in the tropospheric SSW precursors of either PDV phase with respect to PDV^N (Fig. 7A–C). The patterns of these differences for PDV⁺ and PDV⁻ have some centers in common. More importantly, these centers are of the same sign for both PDV phases, that is, positive Z500 anomalies over Eastern Asia and negative anomalies over North America are located close to the main precursory structures. Consequently, Figure 7A implies that the intensification of the SSW precursors found for PDV⁺ (Fig. 3A) is weaker than that expected by a linear PDV⁺ impact. Conversely, Figure 7B indicates that the weakening of SSW precursors found for PDV⁻ (Fig. 3B) is boosted through a nonlinear PDV⁻ impact. By contrast, in the case of the tropospheric response to SSWs during either PDV phases (Fig. 7D and E) and for SSW-related tropospheric anomalies during AMV phases (Fig. 7G–L), the PDV and AMV modulations are instead essentially linear. The modulation of SSW-related anomalies is, indeed, negligible when the AMV influence is removed, except for small regions.

Conclusions and discussion

The multidecadal variability of SSWs and its sources have received little attention from the scientific community so far, as it requires a long daily data record at stratospheric levels that are typically not available in observations and model simulations. In this study, we take advantage of one of the most recent large ensembles (MPI-GE) of historical experiments performed with a high-top model (MPI-ESM1.1) to investigate the influence of mul-

tidecadal SST variability on SSWs. In particular, we focus on the main low-frequency variability of the Pacific and Atlantic oceans, the PDV and AMV, respectively.

The main conclusions drawn from our study can be summarized as follows:

- The frequency of SSWs in winter is modulated by the PDV but not by the AMV. In particular, the PDV⁺ phase shows statistically significantly higher frequency of SSWs compared with PDV⁻ and PDV^N conditions. This PDV influence is largest in January, and it is independent of the phase of the AMV.
- The precursor and response patterns of SSWs are affected by the PDV and AMV mostly in their respective ocean basin of influence, and the signal in the other basin is mainly due to the aliasing of the AMV and PDV phases of opposite sign. The modulation of SSW precursors is larger than that of the response to SSWs, particularly in the case of the PDV.
- The main tropospheric precursor of the SSW (an anomalous Northwestern Pacific low) is enhanced and eastward shifted over the Pacific during PDV⁺. The opposite occurs during PDV⁻.
- The PDV modulation of the tropospheric response to SSWs is similar to the annular mode pattern but with the strongest centers of action over the Pacific. The AMV instead leads to a strong modulation of this response over the North Atlantic.
- The changes in the frequency of SSWs due to the PDV might be explained by the PDV modulation of the background tropospheric state in the North Pacific, which is a key region for SSW precursors. This modulation is achieved by constructive interference with stationary WN1 wave activity. By contrast, such modulation is not found for the AMV.

Apart from multidecadal oceanic variability, we acknowledge that there might be other sources of long-term SSW variability, such as multidecadal variability in the amplitude of the QBO⁸ or ENSO. As previously mentioned, a QBO is not present in the MPI-GE because of the relatively low vertical resolution of this version of the atmospheric model. New simulations with a model version with

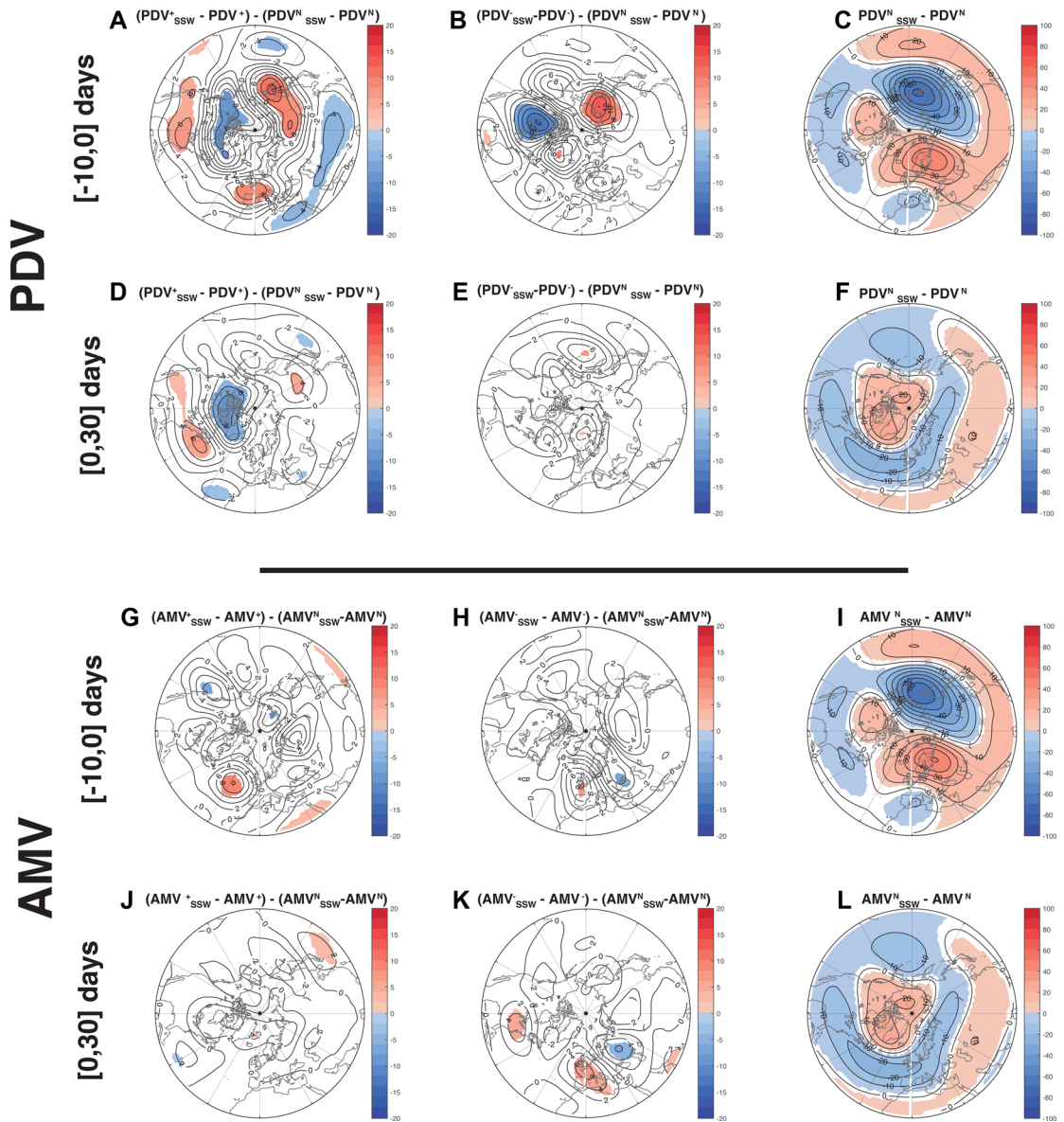


Figure 7. Linearity of PDV/AMV influences on the mean atmosphere and tropospheric precursors and impacts of SSWs. Composite maps of detrended 8-day low-pass filtered geopotential height anomalies at 500 hPa (Z500) for [−10,0] days before SSWs (panels A–C and G–I) and for [0,30] days after SSWs (panels D–F and J–L). Anomalies are computed with respect to the particular SST state, and so labeled: $PDV^+_{SSW}-PDV^+$, $PDV^-_{SSW}-PDV^-$, and so on, where the averages for days before and after SSWs are denoted by the subscript “SSW” to differentiate from the non-SSW stratified averages. (A and B) Difference between anomalies for $(PDV^+_{SSW}-PDV^+)$ minus $(PDV^N_{SSW}-PDV^N)$, and for $(PDV^-_{SSW}-PDV^-)$ minus $(PDV^N_{SSW}-PDV^N)$, respectively. (C) $PDV^N_{SSW}-PDV^N$ anomaly. (D–F) Same as (A–C) but for [0,30] days after SSWs. Shading indicates statistically significant values at a 95% confidence level. Contour interval: 5 m (A, B, D, and E) and 10 m (C and F). (G–L). Same as (A–F) but for the AMV.

higher vertical resolution would be needed to obtain a QBO and perform such an analysis. On the other hand, some observational studies have documented the multidecadal variability of some ENSO features,

such as its impact on the Euro-Atlantic sector with a contribution of the stratospheric state.⁴⁶ However, their short observational data record hampered to draw robust conclusions. In our analysis, the ENSO

signal has been removed, but the MPI-GE gives the opportunity to revisit in the future this and other similar open questions.

It is important to note that our analysis only focuses on the direct effects of the multidecadal oceanic variability on the atmosphere and, consequently, on the occurrence of SSWs. Interestingly, several very recent studies have already established a possible effect of AMV and/or PDV on Arctic sea ice,^{47–49} and some others have even suggested that the PDV can regulate the contribution of sea ice loss to Arctic amplification.⁵⁰ Since changes in sea ice have been shown to impact tropospheric, and more importantly for our study, stratospheric circulation (e.g., Ref. 51 and 52), it could then be worthwhile to investigate further whether these PDV- and/or AMV-induced sea ice changes are a large part of the effects of this multidecadal oceanic variability on the stratosphere.

Overall, our results agree with most previous studies regarding the effects of PDV on polar stratospheric circulation (e.g., Refs. 9–11), although these works analyzed the impact of the full PDV signal, while we focus here on decadal and longer timescales. Only Ref. 12 studied the impact of the decadal PDV signal. Interestingly, they found opposite stratospheric responses when using the filtered and unfiltered PDV, while we do not. They explain this opposite response through changes in the atmospheric background state, which modifies the wave propagation from the troposphere to the stratosphere. However, it is important to note that they used either a relatively short observational data record or a low-top model (CAM5), while we employ a high-top model with a well-resolved stratosphere, and so, it is possible that the simulation of the stratospheric state shows substantial differences. Another advantage of our study is the long record we used, which allows us to obtain a statistically significant PDV impact on SSWs. Ref. 11, for instance, also identified an enhanced (reduced) SSW frequency during PDV⁺ (PDV⁻) but was not statistically significant. In addition to changes in the frequency of SSWs, the long daily output allowed us to explore the modulation of tropospheric precursors and response to SSWs by PDV.

Regarding the AMV, our results are consistent with the previous work^{15,17,18,19} on the modulation of the tropospheric background state. Refs. 17–19 detected a weakening of the polar vortex, while

our analysis does not reveal a clear signal. The discrepancy is probably due to the winter months selected, as these authors document the significant AMV impact on the stratosphere for early winter (November–December), while we focus on DJF. In addition, one of these studies, Ref. 19, finds an opposite signal in the stratosphere between early winter and midwinter (January–February), so doing a DJF average in this study may cancel out the anomalies. Concerning the AMV influence on SSWs, Ref. 15 found an increase of around 10% in the frequency of SSWs for AMV⁺, whereas we do not detect a significant change in the occurrence of SSWs associated with the AMV. Nevertheless, it is important to note that these authors did not provide information about the statistical significance of this result, and more importantly, they did not use transient simulations where AMV-related SST anomalies in other basins were included, as we did. Although no significant effects of AMV are found in the occurrence and triggering of SSWs, the finding on the modulation of the tropospheric response to SSWs is novel and extremely relevant for both the stratospheric and tropospheric communities. Not all SSWs have a visible downward impact,^{6,35,53} and the full prediction of this downward impact is still not possible.² In this study, we have already sub-selected the SSWs to include those with the most likely downward impact³⁵ due to the long persistence of stratospheric anomalies. Nevertheless, here, we show that the tropospheric response to this subset of SSWs is modulated by the AMV, in such a way that it can be significantly weakened owing to the AMV⁻ fingerprint. Thus, our results can help to improve the conditional predictions of the SSW signal in the troposphere. Indeed, these results for the AMV and those obtained for the PDV can be extremely helpful for improving not only subseasonal but also decadal predictions over the Northern Hemisphere middle and high latitudes.

Acknowledgments

B.A. and N.C. were supported by the Spanish Ministry of Science, Innovation and Universities through the JeDiS (RTI2018-096402-B-I00) project. This research is part of POLARCSIC activities. E.M. and D.M. acknowledge the support of the German Federal Ministry of Education and Research through the JPI Climate/JPI Oceans NextG-Climate Science-ROADMAP (FKZ: 01LP2002A) Project,

and of the European Union's Horizon 2020 Programme through the Blue-Action Project, Grant Agreement No. 727852. We are grateful to Mikhail Dobrynin for having conducted the MPI-ESM historical experiments with daily outputs, to Alexey Karpechko for discussion on SSW definitions, and to Evangelos Tyrlis for the MPI internal review. The simulations were performed at the facilities of the German Climate Computing Centre (DKRZ). For the analysis, we acknowledge the use of resources from the bm0966 and bm1190 projects.

Author contributions

B.A. and E.M. led the analysis and carried out the analysis of the model output. N.C. and D.M. also contributed to the design of the analysis. All authors interpreted the results and wrote the paper.

Competing interests

The authors declare no competing interests.

References

- Andrews, D.G., J.R. Holton & C.B. Leovy. 1987. *Middle Atmosphere Dynamics*. Orlando, FL: Academic Press.
- Baldwin, M.P., B. Ayarzagüena, T. Birner, *et al.* 2021. Sudden stratospheric warmings. *Rev. Geophys.* **58**: <https://doi.org/10.1029/2020RG000708>.
- Reichler, T., J. Kim, E. Manzini, *et al.* 2012. A stratospheric connection to Atlantic climate variability. *Nat. Geosci.* **5**: 783–787.
- Smith, K.L., L.M. Polvani & L.B. Tremblay. 2018. The impact of stratospheric circulation extremes on minimum Arctic sea ice extent. *J. Clim.* **31**: 7169–7183.
- Butler, A.H., D.J. Seidel, S.C. Hardiman, *et al.* 2015. Defining sudden stratospheric warmings. *Bull. Am. Meteor. Soc.* **96**: 1913–1928.
- Domeisen, D.I.V. 2019. Estimating the frequency of sudden stratospheric warming events from surface observations of the North Atlantic Oscillation. *J. Geophys. Res.* **124**: 3180–3194.
- Schimanke, S., J. Körper, T. Spanghel & U. Cubasch. 2011. Multi-decadal variability of sudden stratospheric warmings in an AOGCM. *Geophys. Res. Lett.* **38**: L01801.
- Dimdore-Miles, O., L. Gray & S. Osprey. 2021. Origins of multi-decadal variability in sudden stratospheric warmings. *Wea. Clim. Dyn.* **2**: 205–231.
- Jadin, E.A., K. Wei, Y.A. Zyuilyaeva, *et al.* 2010. Connection between stratospheric vortex events and the Pacific Decadal Oscillation. *J. Atmos. Sol-Terr. Phys.* **72**: 1163–1170.
- Woo, S.-H., M.-K. Sung, S.-W. Son & J.-S. Kug. 2015. Connection between stratospheric vortex events and the Pacific Decadal Oscillation. *Clim. Dyn.* **45**: 3481–3492.
- Kren, A.C., D.R. Marsh, A.K. Smith & P. Pilewskie. 2016. Wintertime Northern Hemisphere response in the stratosphere to the Pacific Decadal Oscillation using the Whole Atmosphere Community Climate Model. *J. Clim.* **29**: 1031–1049.
- Hu, D. & Z. Guan. 2018. Decadal relationship between the stratospheric Arctic vortex and Pacific Decadal Oscillation. *J. Clim.* **31**: 3371–3386.
- Hurwitz, M.M., P.A. Newman & C.I. Garfinkel. 2011. The Arctic vortex in March 2011: a dynamical perspective. *Atmos. Chem. Phys.* **11**: 11447–11453.
- Hurwitz, M.M., P.A. Newman & C.I. Garfinkel. 2012. On the influence of North Pacific sea surface temperature on the Arctic winter climate. *J. Geophys. Res.* **117**: D19110.
- Elsbury, D., Y. Peings, D. Saint-Martin, *et al.* 2019. The atmospheric response to positive IPV, positive AMV, and their combination in boreal winter. *J. Clim.* **32**: 4193–4213.
- Newman, M. *et al.* 2016. The Pacific Decadal Oscillation, revisited. *J. Clim.* **29**: 4399–4427.
- Omrani, N.-E., N.S. Keenlyside, J. Bader & E. Manzini. 2014. Stratosphere key for wintertime atmospheric response to warm Atlantic decadal conditions. *Clim. Dyn.* **42**: 649–663.
- Omrani, N.-E., J. Bader, N.S. Keenlyside & E. Manzini. 2016. Troposphere–stratosphere response to large-scale North Atlantic Ocean variability in an atmosphere/ocean coupled model. *Clim. Dyn.* **46**: 1397–1415.
- Peings, Y. & G. Magnusdottir. 2016. Wintertime atmospheric response to Atlantic multidecadal variability: effect of stratospheric representation and ocean–atmosphere coupling. *Clim. Dyn.* **47**: 1029–1047.
- Li, F., Y.J. Orsolini, H. Wang, *et al.* 2018. Modulation of the Aleutian–Icelandic low seesaw and its surface impacts by the Atlantic Multidecadal Oscillation. *Adv. Atmos. Sci.* **35**: 95–105.
- Maher, N., S. Milinski, L. Suarez-Gutierrez, *et al.* 2019. The Max Planck Institute Grand Ensemble: enabling the exploration of climate system variability. *J. Adv. Mod. Earth Sys.* **11**: 2050–2069.
- Giorgetta, M.A., J. Jungclaus, C.H. Reick, *et al.* 2013. Climate and carbon cycle changes from 1850 to 2100 in MPI-ESM simulations for the Coupled Model Intercomparison Project Phase 5. *J. Adv. Mod. Earth Sys.* **5**: 572–597.
- Giorgetta, M.A., E. Manzini, E. Roeckner, *et al.* 2006. Climatology and forcing of the quasi-biennial oscillation in the MAECHAM5 model. *J. Clim.* **19**: 3882–3901.
- Taylor, K.E., R.J. Stouffer & G.A. Meehl. 2012. An overview of CMIP5 and the experiment design. *Bull. Am. Meteor. Soc.* **93**: 485–498.
- Cionni, I., V. Eyring, J.F. Lamarque, *et al.* 2011. Ozone database in support of CMIP5 simulations: results and corresponding radiative forcing. *Atmos. Chem. Phys.* **11**: 11267–11292.
- Stenchikov, G.L., I. Kirchner, A. Robock, *et al.* 1998. Radiative forcing from the 1991 Mount Pinatubo volcanic eruption. *J. Geophys. Res.* **103**: 13837–13857.
- Bittner, M., H. Schmidt, C. Timmreck & F. Sienz. 2016. Using a large ensemble of simulations to assess the Northern Hemisphere stratospheric dynamical response to tropical volcanic eruptions and its uncertainty. *Geophys. Res. Lett.* **43**: 9324–9332.
- Gerber, E.P., M.P. Baldwin, H. Akiyoshi, *et al.* 2010. Stratosphere–troposphere coupling and annular mode

- variability in chemistry-climate models. *J. Geophys. Res.* **115**: D00M06.
29. Nishii, K., H. Nakamura & Y.J. Orsolini. 2011. Geographical dependence observed in blocking high influence on the stratospheric variability through enhancement and suppression of upward planetary-wave propagation. *J. Clim.* **24**: 6408–6423.
 30. Kodera, K., K. Matthes, K. Shibata, *et al.* 2003. Solar impact on the lower mesospheric subtropical jet: a comparative study with general circulation model simulations. *Geophys. Res. Lett.* **30**: 1315.
 31. Trenberth, K.E. & D.J. Shea. 2006. Atlantic hurricanes and natural variability in 2005. *Geophys. Res. Lett.* **33**: L12704.
 32. Charlton, A.J. & L.M. Polvani. 2007. A new look at stratospheric sudden warmings. Part I: climatology and modeling benchmarks. *J. Clim.* **20**: 449–469.
 33. Schmidt, H., S. Rast, F. Bunzel, *et al.* 2013. Response of the middle atmosphere to anthropogenic and natural forcings in the CMIP5 simulations with the Max Planck Institute Earth system model. *J. Adv. Model. Earth Syst.* **5**: 98–116.
 34. Kim, J., S.-W. Son, E.P. Gerber & H.-S. Park. 2017. Defining sudden stratospheric warming in climate models: accounting for biases in model climatologies. *J. Clim.* **30**: 5529–5546.
 35. Karpechko, A.Y., P. Hitchcock, D.H.W. Peters & A. Schneider. 2017. Predictability of downward propagation of major sudden stratospheric warmings. *Q. J. R. Meteorol. Soc.* **143**: 1459–1470.
 36. Mantua, N.J., S.R. Hare, Y. Zhang, *et al.* 1997. A Pacific interdecadal climate oscillation with impacts on salmon production. *Bull. Am. Meteor. Soc.* **78**: 1069–1080.
 37. Wilks, D.S. 2011. *Statistical Methods in the Atmospheric Sciences*. 3rd ed. Academic Press.
 38. Nelson, L.S. 1989. Evaluating overlapping confidence intervals. *J. Qual. Technol.* **21**: 140–141.
 39. Zhang, R. & T.L. Delworth. 2007. Impact of the Atlantic Multidecadal Oscillation on North Pacific climate variability. *Geophys. Res. Lett.* **34**: L23708.
 40. Meehl, G.A., A. Hu, F. Castruccio, *et al.* 2021. Atlantic and Pacific tropics connected by mutually interactive decadal-timescale processes. *Nat. Geosci.* **14**: 36–42.
 41. Garfinkel, C.I., D.L. Hartmann & F. Sassi. 2010. Tropospheric precursors of anomalous Northern Hemisphere stratospheric polar vortices. *J. Clim.* **23**: 3282–3299.
 42. Limpasuvan, V., D.W.J. Thompson & D.L. Hartmann. 2004. The life cycle of the Northern Hemisphere sudden stratospheric warmings. *J. Clim.* **17**: 2584–2596.
 43. Ayarzagüena, B., F.M. Palmeiro, D. Barriopedro, *et al.* 2019. On the representation of major stratospheric warmings in reanalyses. *Atmos. Chem. Phys.* **19**: 9469–9484.
 44. Barnston, A.G. & R.E. Livezey. 1987. Classification, seasonality and persistence of low-frequency atmospheric circulation patterns. *Mon. Wea. Rev.* **115**: 1083–1126.
 45. Smith, K.L. & P.J. Kushner. 2012. Linear interference and the initiation of extratropical stratosphere–troposphere interactions. *J. Geophys. Res.* **117**: D13107.
 46. Ayarzagüena, B., J. López-Parages, M. Iza, *et al.* 2019. Stratospheric role in interdecadal changes of El Niño impacts over Europe. *Clim. Dyn.* **52**: 1173–1186.
 47. Zhang, R. 2015. Mechanisms for low-frequency variability of summer Arctic sea ice extent. *Proc. Natl. Acad. Sci. USA* **112**: 4570–4575.
 48. Castruccio, F.S., Y. Ruprich-Robert, S.G. Yeager, *et al.* 2019. Modulation of Arctic sea ice loss by atmospheric teleconnections from Atlantic multidecadal variability. *J. Clim.* **32**: 1419–1441.
 49. Kim, H., S.-W. Yeh, S.-I. An & S.-Y. Song. 2020. Changes in the role of Pacific decadal oscillation on sea ice extent variability across the mid-1990s. *Sci. Rep.* **10**: 17564.
 50. Screen, J.A. & J.A. Francis. 2016. Contribution of sea-ice loss to Arctic amplification is regulated by Pacific Ocean decadal variability. *Nat. Clim. Change* **6**: 856–861.
 51. Cohen, J. *et al.* 2014. Recent Arctic amplification and extreme mid-latitude weather. *Nat. Geosci.* **7**: 627–637.
 52. Sun, L., C. Deser & R.A. Thomas. 2015. Mechanisms of stratospheric and tropospheric circulation response to projected Arctic sea ice loss. *J. Clim.* **28**: 7824–7845.
 53. Charlton-Perez, A.J., L. Ferranti & R.W. Lee. 2018. The influence of the stratospheric state on North Atlantic weather regimes. *Q. J. R. Meteorol. Soc.* **144**: 1140–1151.